CrossMark

Method for the Enhancement of Buildability and Bending Resistance of 3D Printable Tailing Mortar

Zhijian Li[1,2], Li Wang[2],*, and Guowei Ma[2,3]

Abstract: The innovative 3D printing has been successfully applied to layeredly build-up construction-scale structures through the extrusion of various cementitious materials. Favourable buildability of fresh cement mixture and the hardened properties of the printed structures are essential requirement for the application of 3D concrete printing. This paper firstly proposed a 3D printable cement mixture containing 40% mining tailings. The influence of paste age on the buildability of forty-layer structure was evaluated, as well as the bending resistance of prism specimen sawed from the printed structure. The bonding between layers is a critical factor that influences the structural capacity. In particular, the weak bonding interface formed in the layered extrusion process was identified through high-resolution X-ray CT scanning. It is necessary and desirable for the cement paste to perform both well buildability and mechanical performances. Thereafter, a proper amount of viscosity modify agent (VMA) was used to improve the structural integrity by increasing the contact behaviour between the adjacent extruded layers. Meanwhile, the impact of curing method on the hardened properties of 3D printed structures was accessed. Results indicated that the prepared tailing mortar achieved sufficient buildability to be used in an extrusion-typed 3D printer at the paste age of 45 min. The mould-cast specimens process flexural strength of 7.87 MPa. In contrast, the flexural strength of printed specimens values 5.22 MPa and 12.93 MPa, respectively, after the addition of 1.5% VMA and 90 °C steam curing.

Keywords: 3D concrete printing, buildability, bending behaviour, weak bonding interface, layered structure.

1. Introduction

In recent few years, various 3D printing techniques have been developed and pave a promising way for the optimal design of complex solid models and the guidance to real engineering practices (Ju et al. 2017a, b). Lots of attempts have been conducted to explore the potential of 3D printing in the building and construction industries, such as D-shape, contour crafting and concrete printing (Buswell et al. 2007; Gibbons et al. 2010; Le et al. 2012; Cesaretti et al. 2014; Kazemian et al. 2017). Such techniques are well suited to the production of one-off, complex structures that would often be difficult to produce using traditional manufacturing methods. Cementitious materials that are compatible with 3D printing promote rapid application of this innovative technique in the construction field with advantages of cost effective, high efficiency, design flexibility and environmental friendly (Khoshnevis 2004; Zhang and Khoshnevis 2013; Labonnote et al. 2016; Attaran 2017). It is critical to ensure a complementary connection between the designs of the printable mix and printing machine. Up to date, various 3D printable mixtures have been continuously developed, such as high-performance composite (Le et al. 2012; Gosselin et al. 2016), fibre reinforced mixtures (Hambach and Volkmer 2017), etc. A number of specific implementation practices have been presented. For example, a five-story apartment 3D printed by WinSun (2015), the BigDelta project (WASP 2016), a castle printed in situ (Rudenko 2015), architectural elements (Gosselin et al. 2016) etc., which have all demonstrated the great potential and feasibility of 3D printing in constructing large-scale building components.

The printable property of fresh cementitious materials and the mechanical behavior of the hardened structures are of great concerns for current 3D printing technologies (Le et al. 2012; Feng et al. 2015; Perrot et al. 2016; Ma and Wang 2017). One of the important printable characteristics is the buildability, which refers to the ability of cement paste to retain its extruded shape under self-weight and the resistance to the pressure from upper layers (Le et al. 2012; Lim et al. 2012; Perrot et al. 2016). Buildability can be considered as the early stage stiffness. Good buildability is a basic requirement for 3D printable mixtures. A feasible approach

[1] College of Architecture and Civil Engineering, Beijing University of Technology, 100 Pingleyuan, Chaoyang District, Beijing 100124, China.

[2] School of Civil Engineering and Transportation, Hebei University of Technology, 5340 Xiping Road, Beichen District, Tianjin 300130, China.

*Corresponding Author; E-mail: wangl1@126.com

[3] School of Civil, Environmental and Mining Engineering, The University of Western Australia, Crawley, WA 6009, Australia.

for improving the buildability is to properly extent the paste age of the mixture (Reinhardt and Grosse 2004; Voigt et al. 2006). A longer time allows the further cement hydration and therefore contributing the mix to acquire certain stiffness.

However, this approach would scarify the fluidity and adhesive behavior of the fresh paste, which may result in poor hardened structural capability and integrity. In the printing process, the concrete components are created by bonding the extruded filaments together to form each layer without using extra formworks (Pegna 1997; Khoshnevis and Dutton 1998; Feng and Liang 2014). The rheology and flowability of the fresh material must allow its fluent extrusion to form small filaments. Concrete paste of low fluidity and adhesion is likely to form voids between filaments and weak bonding interface between adjacent filament and layers, which are negative for the overall mechanical performances (Le et al. 2012). Therefore, it is of great significance for the cement paste to optimize and coordinate the well buildability and mechanical properties.

Proper treatment can be applied to improve the bonding between the layers and to decrease the voids formed by the filaments. Viscosity modifying agents (VMA) are water soluble polymers that control the flow characteristics and rheological performance of concrete mortars (Lachemi et al. 2004; Leemann and Winnefeld 2007; Benaicha et al. 2015). VMA is also a good material to ensure extrudability as it reduces the cement paste permeability, and therefore reduces the less risk of water drainage (Perrot et al. 2006, 2012, 2015). Research investigations have indicated that adding VMA in cement pastes decreases the flowability at a constant water content, however, it can increase corresponding yield stress and plastic viscosity (Leemann and Winnefeld 2007; Benaicha et al. 2015). Proper addition of VMA can improve the water retention and reduce the bleeding, contributing to the contact and bonding between the adjacently deposited filaments. The overall mechanical properties are therefore enhanced (Kovler and Jensen 2005; Lin and Huang 2010). It is therefore feasible and promising to improve the bonding effect of extruded layers by incorporating proper dosage of VMA. Besides, the 3D printing process of construction differs from the traditionally fabrication process. This innovative technique is appropriate for pre-fabricated structural components. Proper curing method can be employed to the hardened structures to improve the degree of cement hydration and the compactness of microstructure of the matrix. However, there is little investigation available regarding to the influence of VMA and post-curing method on the viscous and bonding property of cement motors used for 3D printing.

The objective of study is to optimize the structural integrity and mechanical performance of the components printed at a favourable buildability situation. To this end, this paper firstly proposed a 3D printable cementitious material that is suitable for the extrusion-based printing process. The influence of paste age on the buildability of fresh motors was evaluated to reach a desirable buildability. Meanwhile, the bending resistance of printed prism specimens fabricated at

different paste ages was tested. Thereafter, a proper amount of viscosity modify agent (VMA) and different curing method were applied to improve the structural capacity by increasing the bonding force between the adjacent extruded layers. Particularly, X-ray CT scanning was implemented to characterize the weak bonding interfaces formed in the layered extrusion processes.

2. Materials and Methods

2.1 Material Preparation
Rapid hardening Portland cement P. O 42.5R, fly ash and silica fume are used as the binding materials. Local river sand with a specific surface area of 0.101 m^2/g and copper tailings with a specific surface area of 0.141 m^2/g serve as the fine aggregates. Besides, high efficient polycarboxylate-based superplasticizer with a water reducing rate of more than 30% and a solid content fraction of 37.2% are adopted to achieve the required flowability for the mixture. Flowability should be controlled to ensure the fresh paste is smoothly and continuously transported from the storage system to the nozzle without blockage and disruption, therefore realizing the compatibility between workability and printing process. Additionally, a low shrinkage is essential as the freeform components are built without formwork. A small amount of polypropylene (PP) fibers are employed to reduce the cracking produced by water evaporation. Table 1 shows the mixture proportions of the raw materials used for material preparation. The chemical compositions of tailing determined by X-ray fluorescence (XRF) analysis are listed in Table 2. Meanwhile, the particle size distribution parameter of tailings is presented in Table 3. After a series of attempts and trials, it was found that the most suitable mix for printing is comprised of a tailing to sand mass ratio of 2:3, which mean that 40% natural sand was replaced by mining tailings (Ma et al. 2018).

In the preparation process, PP fibers and the dry powders, i.e., cement, fly ash, silica fume, natural sand and tailings are firstly mixed and blended for three minutes to obtain a uniform mixture. Then, one half of the total amount of water along with the superplasticizer is added in and stirred for 2 min. Subsequently, the second half of the total amount of water together with superplasticizer is poured in and stirred for an additional two minutes.

2.2 Prism Specimen Manufacture
After the blending, fresh paste is delivered to the material storage tank equipped in our self-designed printing system to manufacture a forty-layer structure. The printed structure is illustrated in Fig. 1(a). It is built-up by vertically stacking extruded filaments of length of 250 mm and width of 30 mm without collapse. The opening of the printing nozzle is 8 mm × 30 mm. After a series of trials, the optimal operational parameters are determined for a smoothly printing process. The extrusion rate V_e of the cementitious material is designed as 5.4 litres/minute and the printing speed V_p is controlled as 450 mm/min. The extrusion rate of fresh

Table 1 Mixture proportions of the raw materials used for 3D printable cementitious material.

Mix no.	Natural sand	Tailings	Replacement (%)	Cement	Fly ash	Silica fume	Water	Superplasticizer (%)	PP fiber (kg/m^3)
R30	0.72	0.48	40	0.7	0.2	0.1	0.27	1.083	1.2

Table 2 Chemical Composition of tailings by mass ratio.

SiO_2	Al_2O_3	Fe_2O_3	CaO	MgO	SO_3	Na_2O	P_2O_5	K_2O	MnO
39.77	4.61	20.16	22.29	7.17	3.05	1.32	0.26	0.44	0.23

Table 3 Particle size distribution parameters for copper tailings.

	d(0.1) (μm)	d(0.5) (μm)	d(0.9) (μm)	Average (μm)
Tailing	38.03	123.75	375.10	24.60

The d(0.1), d(0.5) and d(0.9) denote the size of the 10, 50 and 90% of the particles measured are smaller than or equal to the size stated.
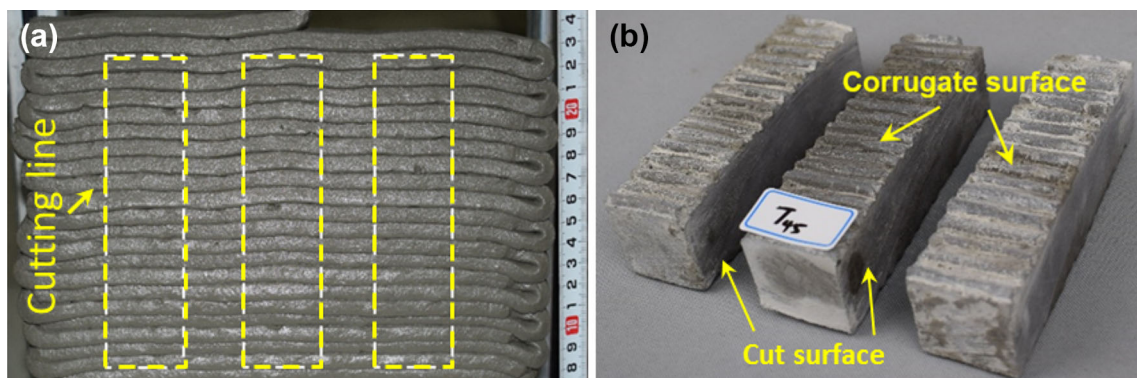
Fig. 1 **a** Forty-layer structure manufactured through an extrusion based printing system and **b** prism specimens with corrugate surface sawed from the printed structure.

mortar is controlled by the rotation of a mixing blade that firmly connected to a drive motor. The speed V_p accounts for the moving speed of the printing nozzle, which is also controlled by a drive motor. More detailed information can refer to our previous experimental investigations (Ma et al. 2018).

Thereafter, prism specimens with size of 30 mm × 30 mm × 120 mm are sawed from the 3D printed structure. As the picture shown in Fig. 1(b), the prism samples are of corrugate surfaces and the layers are perpendicular to printing direction. Then the printed specimens are smoothed to eliminate the influence of corrugate surface on the fracture behaviours, since that cracks are prone to initiate from the transition zones between two layers. Meanwhile, specimens manufactured in mould-cast state are taken as the reference specimens.

2.3 Testing Procedure

Table 4 presents the testing procedures which are designed to find out an optimal solution for the 3D printable mortar to reach a favourable buildability and structural capacity. Flexural behaviours are investigated in both mould-cast and printed specimens. Herein, three factors are considered, i.e. paste age, VMA dosage and curing method.

Paste age refers to the duration from the ending of the blending of raw materials to the starting of the printing. The liquid and viscous property of fresh pastes are crucial to the bonding performance between layers, which greatly depends on the paste age. It is expected that the shorter the paste age, the higher bonding strength between layers. Three paste ages range from 15 to 45 min and three VMA contents range in 0.5–1.5% are taking into account. A longer paste age was not considered due to the fresh mortar became stiff and then could not be printed. Once the specimens are demoulded after 24-h curing at room temperature, they are cured by three different methods to monitor the strength development with time. The water curing method is designed to directly immerse the specimens into water at room temperature (approximately 20 °C) for 7 days. The steam curing method is to cure the samples with steam at 90 °C for 72 h. While the standard curing method is to place the samples in the moist cabinet for proper curing with an ambient temperature of 20 ± 1 °C and the relative humidity of 95 ± 5% for 7 days.

As the testing procedures given in Table 4, series No. T1-T3 are designed to evaluate the influence of paste age on the flexural performance of printed specimens, No. T4–T6 are applied to measure the impact of VMA on the flexural

Table 4 Testing procedures designed for the evaluation of bending resistance.

Series No.	Curing method	Paste age	Viscosity modify agent (%)
T0	Standard curing	Casting	0
T1	Standard curing	15 min	0
T2	Standard curing	30 min	0
T3	Standard curing	45 min	0
T4	Standard curing	45 min	1.0
T5	Standard curing	45 min	1.5
T6	Standard curing	45 min	2.0
T7	Water curing	45 min	0
T8	90 Steam curing	45 min	0
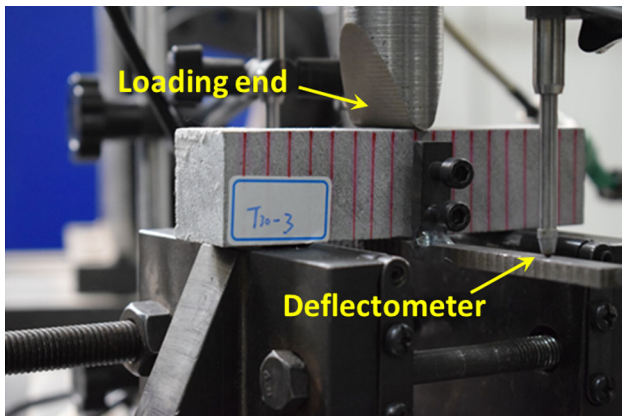
Fig. 2 Set up for three-point bending test.

behaviors, and T3 and T7–T8 are used to access the effect of curing method on the flexural performances. The flexural properties of both printed and casted specimens were tested according to ASTM C348-14 (ASTM 2014). As shown in Fig. 2, a three-point bending jig was mounted on a digital servo-control universal testing machine with a loading capacity of 100 kN to measure the flexural tensile strength. A symmetrical three-point loading setup, with a beam span of 70 mm, was used for the flexural tests. The loading rate was set to 48 N/s. The load–displacement curves for all specimens were automatically recorded until specimen failure. At least three identical specimens for each situation were tested.

2.4 X-ray CT Characterization

Non-destructive X-ray computed tomography (CT) has been widely adopted to provide an accurate identification of the meso/microscopic structure of engineering materials (Lu et al. 2006; Gallucci et al. 2007; Zhang et al. 2012). In this section, we intend to employ the advanced CT technology to detect the voids and weak bonding interfaces formed by the filaments as well as the relative position between the fracture path and interfaces. For scanning, a high-resolution CT with a maximum spatial resolution of 10 μm was adopted, which satisfied the needs of reconstructing meso-level structures. Due to the specimen was beam-shaped, the scanning was

focus on the zones in neighbourhood of the fracture surfaces rather than the whole specimen, aiming to improve the clearness of the detecting images. Moreover, the separated two parts of prism sample after bending test are assembled together to facilitate the CT characterization.

3. Results and Discussion

3.1 Effect of Paste Age on the Buildability

In the section, the influence of paste age on both the buildability and mechanical property are measured and evaluated in order to find an optimal balance between the buildability and strength. To evaluate the influence of paste age on the buildability of fresh mortar paste, 20-layer structures are built up by the proposed tailing mortar at the paste age of 15, 30, and 45 min, respectively. Figure 3 presents the constructed structures with designed dimensions of 30 mm (W) × 250 mm (L) × 160 mm (H). The printed structures illustrate that the fresh mortar material can be stably stacked in the vertical direction without collapse, indicating an acceptable buildability. However, there may form apparent interfaces between adjacent layers due to the inherent layer structure, which is negative to the structural integrity of the 3D printed models.

A longer paste age of the cement-based materials promote the hydration degree of binding materials, and it facilitate the fresh paste turns to plastic state from the fluidity state (Boumiz et al. 1996; Voigt et al. 2003; Trtnik et al. 2008). As the measured data presented in Fig. 4, the height of the structures stacked by a certain number of layers of filaments increases with the paste age. Similarly, the average layer thickness also increases with the paste age. Therefore, the increased stiffness contributes to the development of the buildability, i.e. the ability of the paste to retain its extruded shape and the ability to sustain the weight of the subsequent layers.

At the paste age of 45 min, the average thickness of layers under pressure of self-weight measures 7.5 mm, accounting for 93.8% of the optimal designed value 8.0 mm. The optimal value is the thickness of the right printed filament

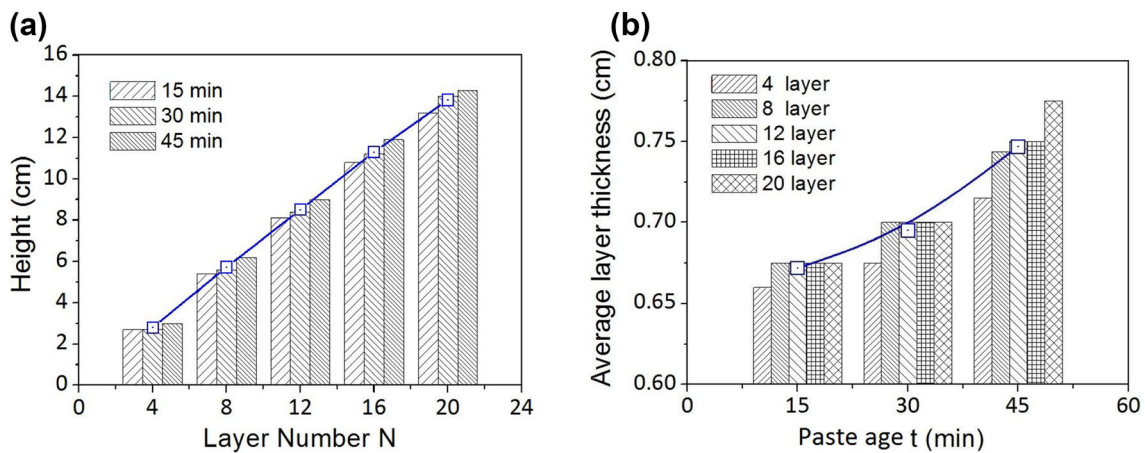**Fig. 3** Structures constructed by the proposed tailing concrete at different paste ages.

Fig. 4 Buildability evaluation of printed structures. **a** Overall height of structures stacked with different number of layers and **b** average layer thickness changes with the paste age.

with no slump. In most cases, it equals to the size of the nozzle. Measured results indicate that the material at the paste age of 45 min can perform favourable loading capacity. Good buildability is featured by a sufficient stiffness and unobvious deformation. It is feasible to improve the buildability by increasing the paste age. However, prolong the paste age will reduce the surface chemical activity to a large extent, produce more voids between two adjacent filaments and form relative weak interfaces between layers, therefore producing negative influences to the mechanical integrity of the printed structures (Panda et al. 2017). In most cases, proper deformation of the filament is expected to fill the voids to improve mechanical capacity of the printed structures through enhancing the contact and bonding of adjacent filaments. Therefore, there is a balancing relationship between the buildability (stiffness) and the void filling (mechanical capacity).

3.2 Effect of Paste Age on the Bending Performance

As above discussed, increasing the buildability through prolong the paste age may scarify the bonding force between adjacent layers. The bending behaviour of prism specimen printed at different paste ages were evaluated.

Figure 5(a) describes the relationship of load (P) and deflection (δ) (displacement in the middle span) of both casted and printed prism specimens in the three-point bending process. From the P-δ curves, all specimens proceeded quickly under load to failure, with the rapid extension of cracks and instantaneous fractures. The P-δ curves displayed no post-peak deformation, indicating obvious brittle failure. Cracking took place in the middle section of the specimens, leading to rough fracture surfaces. The variations in the 7-day flexural strength (f_{flx}) and ultimate deflection (δ_{ult}) in the span centres of the prism specimens printed at different paste ages are presented in Fig. 5(b) and (c), respectively. The flexural strength f_{flx} of specimens printed at the paste age of 15, 30, 45 min was approximately 31.4, 33.4, and 46.1% lower than the casted samples, respectively. Meanwhile, the mid-span defection δ_{ult} of specimens printed at the paste age of 15, 30, 45 min was approximately 49.5, 40.1, and 36.2% lower than the mould-casted samples, respectively. The longer the paste age, the lower the bending resistance. Additionally, the fracture energy G_f was calculated based on the load–deflection curves. G_f quantifies the energy necessary to create a unit area of crack surface projected onto the plane parallel to the crack direction (Zhao et al. 2008). The weak bonded
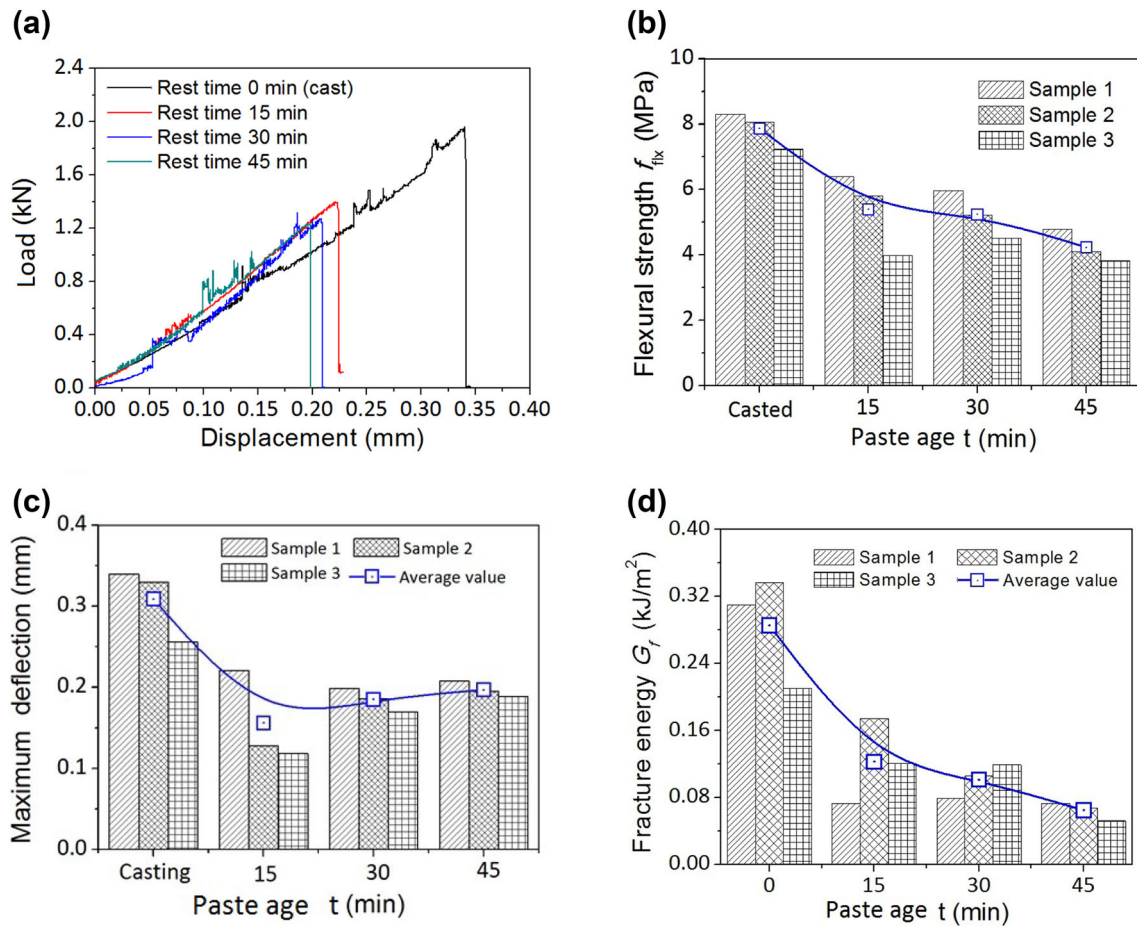
Fig. 5 Evaluation of the bending behaviours. a Load–deflection curves, b flexural strength, c peak-load deflection, and d fracture energy of casted and printed prism specimens.

interfaces of printed specimens are prone to produce cracks and resulting in low fracture energy. As the data shown in Fig. 5(d), the printed structures perform lower crack resistance to the applied bending load. From these test results, in general, the printed specimens are of lower bending/fracture resistance relative to the casted ones, which was mainly derived from the bonding strength between adjacent layers are weaker than that of the matrix mass.

There will form rough fracture surfaces once the specimen failed in the bending loads. The two separated parts are assembled together as Fig. 6 shown to facilitate the CT scanning. Figure 7 illustrates the X-ray CT characterization of microscale structures of prism specimen in neighbourhood of the bending fractures. As the CT images shown in Fig. 7(a), there is no obvious voids other than the intrinsic pores formed in the hydration process. The paste age of 15 min produces a trivial impact on the mortar matrix.

However, the layered structure and significant porosity in the micron order can be seen clearly when the paste age prolonged to 30 min and 45 min, which are characterized by a series of microscale voids/pores, as the pictures displayed in Fig. 7(b) and (c). These voids possess comparative size to the intrinsic pores in the cement matrix. A distinct feature is that they are discontinuously distributed along the boundary of the extruded filaments, as the yellow imaginary line marked in the CT images. From a mesoscopic point, the curved boundary may have induced by the instability of the material extrusion through the small nozzle. The weak interface becomes more noticeable as the paste age increases. The voids located at the boundary of layers demonstrate the existence of the interfaces. Due to the reduction of chemical activity and rheology of the extruded paste, there must be certain discontinuity between the interlayers. However, the poor bonded interfaces will not all certainly
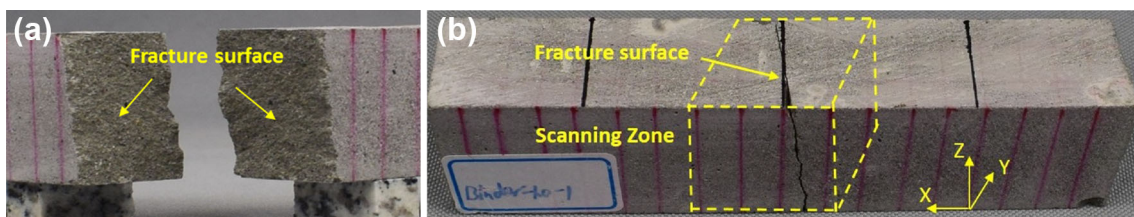
Fig. 6 a Rough surfaces formed after the failure of prism specimen at bending test and b illustration of the CT scanning zone.
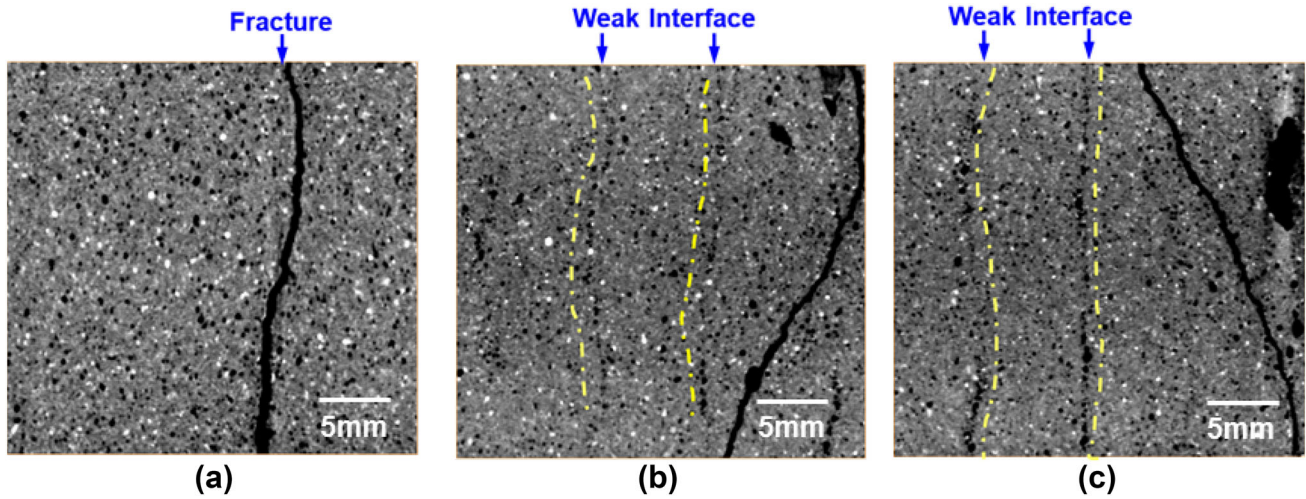
Fig. 7 Microscale characterization of structures in neighbourhood of the bending fractures through X-ray CT scanning. **a–c** Corresponds to one arbitrary XY cross-section of specimens fabricated at the paste age of 15, 30 and 45 min, respectively.

have displayed by a line of voids. Under some conditions, the surfaces are flat contacted and there are not distinct micro-voids produced in the interstices between the filaments. Even though the hardened properties of mortar are likely to be impact by the layered structure and sometimes may result in certain mechanical anisotropy.

3.3 Effect of VMA on the Flowability

The 3D printing process of construction differs from the traditionally fabrication process. The failure modes or the path of the fracture surface is heavily influenced by the layer delamination. The bond strength between stacking layers shall rely on certain specific treatment methods. It is expected that VMA is a proper agent to modify the contact behaviour of two adjacent layers due to its potentiality of water retention and surface tension reduction. However, incorporating a certain amount of VMA into the cementitious mixture may lower the flowability of the fresh material. Figure 8 depicts the fluidity of proposed tailing mortar with different VMA contents. The fluidity is characterised by the

spreading diameter of fresh paste through a vibrate table test, which is introduced in the previous work (Ma et al. 2018). The measured results indicate that, as predicted, the higher VMA content, the more viscous and the lower flowability of cement paste. Based on our previous measurement, the mortar material that keeps a spreading diameter ranging in 17.4–21 cm performs acceptable printability (Ma et al. 2018). As the data presented in Fig. 8, the cement pastes with designed content of VMA (0–1.5%) all keep a spreading diameter within the recommended range and therefore meet the requirement for printing. However, more addition of VMA is not applicable for the fresh mixtures to acquire acceptable printability due to the mortar with low flowability may block the material transition system or even cannot be printed.

3.4 Effect of VMA on the Bending Behaviour

It is expected that the bonding property of the extruded layers will be improved through using a certain amount of VMA. To verify this expectation, the bending behaviour of
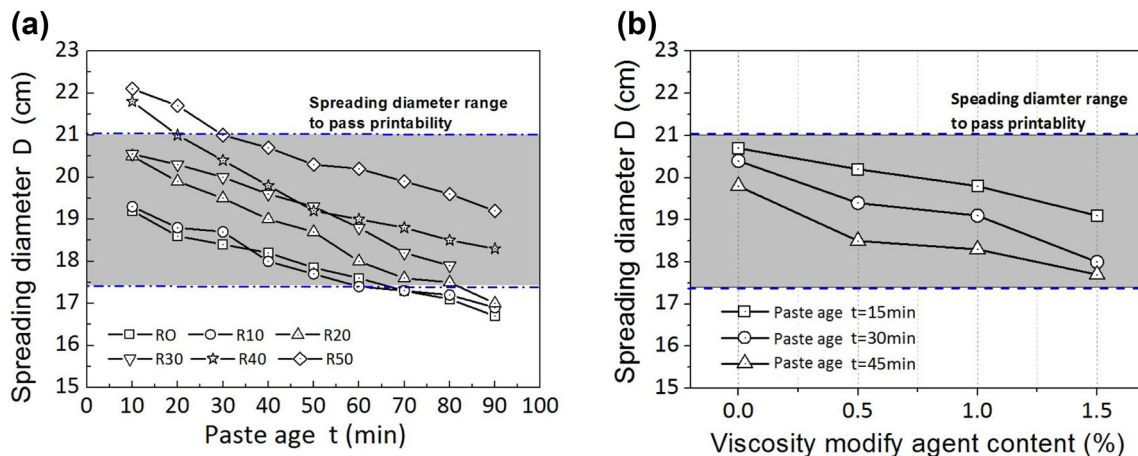
Fig. 8 **a** Spreading diameter range for acceptable printability and **b** relationship between fluidity and the VMA content of cement paste at different paste ages.
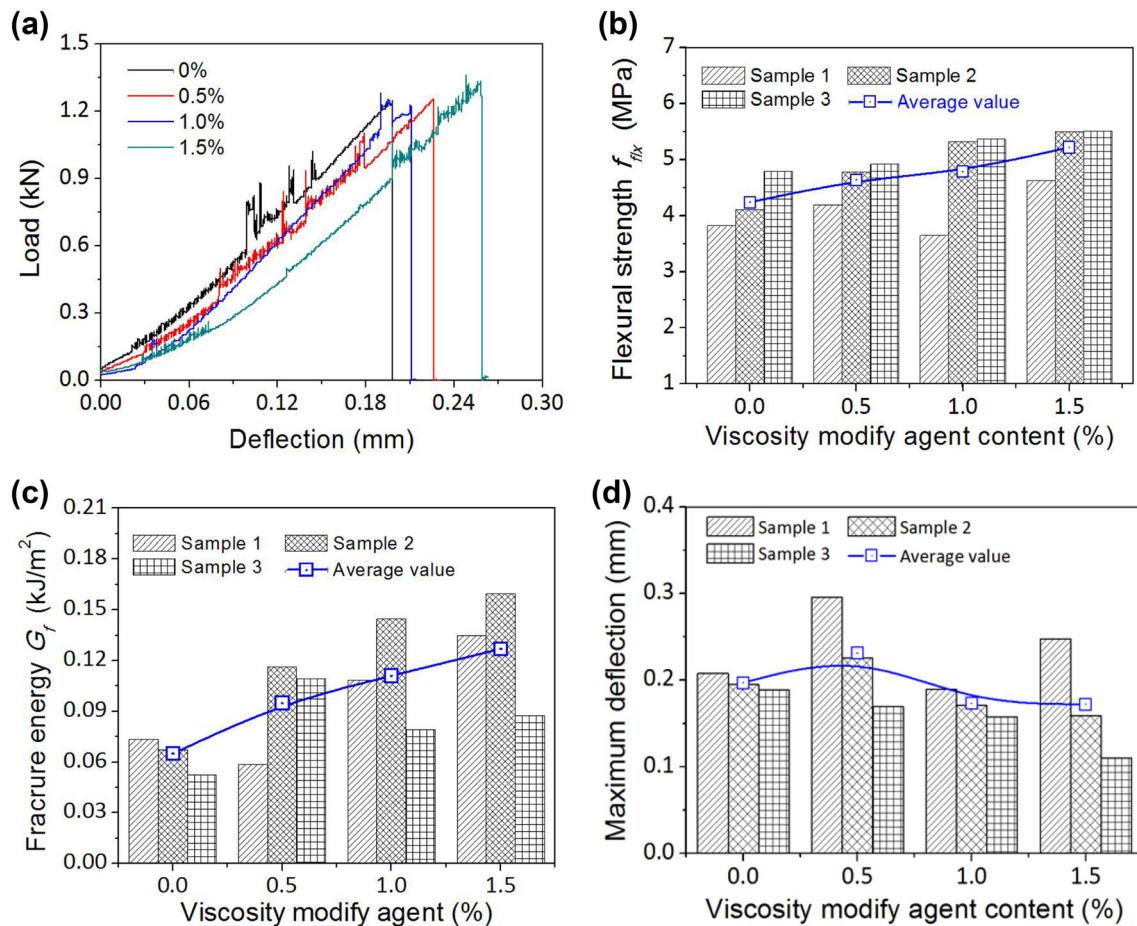
Fig. 9 Evaluation of the bending behaviours. **a** Load–deflection curves, **b** flexural strength, **c** fracture energy, and **d** maximum deflection of printed prism specimens.

prism specimens fabricated with different VMA content was investigated. The paste age for printing is designed at 45 min because of the mixture can acquire favourable buildability at this time. The load–deflection curves of printed specimens with different VMA content are shown in Fig. 9(a). The results indicate that the prism specimens all perform obvious brittleness. The VMA does not produce obvious influence on the failure patterns of printed structures. As the data presented in Fig. 9(b), the flexural strength increases with the addition of VMA and the strength of samples with 1.5% VMA is approximately 26% higher than that without VMA. The results demonstrate the positive contribution of VMA to the mechanical property of printed structures. Meanwhile, the addition of VMA greatly enhanced the fracture resistance. As illustrated in Fig. 9(c), the G_f was improved by 17.6, 42.6, 54.5%, respectively, when 0.5, 1.0 and 1.5% VMA was employed. However, 3D printed beams show no obvious variation of the maximum deflection with the increasing amount of VMA, as shown in Fig. 9(d). Generally, the mechanical properties between adjacently extruded layers were effectively improved through incorporating a certain amount of VMA.

To further probe the influence of VMA on the contacting behaviour between the filaments, CT scanning technique was implemented to characterize the microscale structures in adjacent to fractured zones of tested samples. The detection

method is same as that illustrated in Fig. 6. From the scanning results, when 0.5% VMA is added, the fracture induced by the applied bending loads propagates along the weak bonding face, as the CT image shown in Fig. 10(a), which proves a negative impact of the bonding interface on the mechanical property of the laminated structure. It is of possibility that the cement pastes without or with low dosage of VMA may exhibit certain bleeding of water, therefore, a relatively thin layer of water will be formed on the outer surface of extruded filaments, which produce negative effect on the contact or bonding between adjacent layers. When the addition of VMA is increased, the induced crack is prone to parallelly or crossed propagate along the interface due to the contact property between filaments is improved to a certain degree. As the detection result illustrated in Fig. 10(b), only a short length of crack is converged with the weak interface when the dosage of VMA is increased to 1.0%. It is therefore expected that the interfaces will produce trivial influence to the structural capacity when the adjacent layers are strongly bonded. The CT image presented in Fig. 10(c) proves this expectation. Cracks extent parallelly to the interface instead of converged with it. The addition of VMA enhance water retention and reduced bleeding of cement pastes, contributing the contact or bonding between printed filaments, and therefore eliminating the influence of the interlayer delamination on the fracture path to a large extent. The fractures
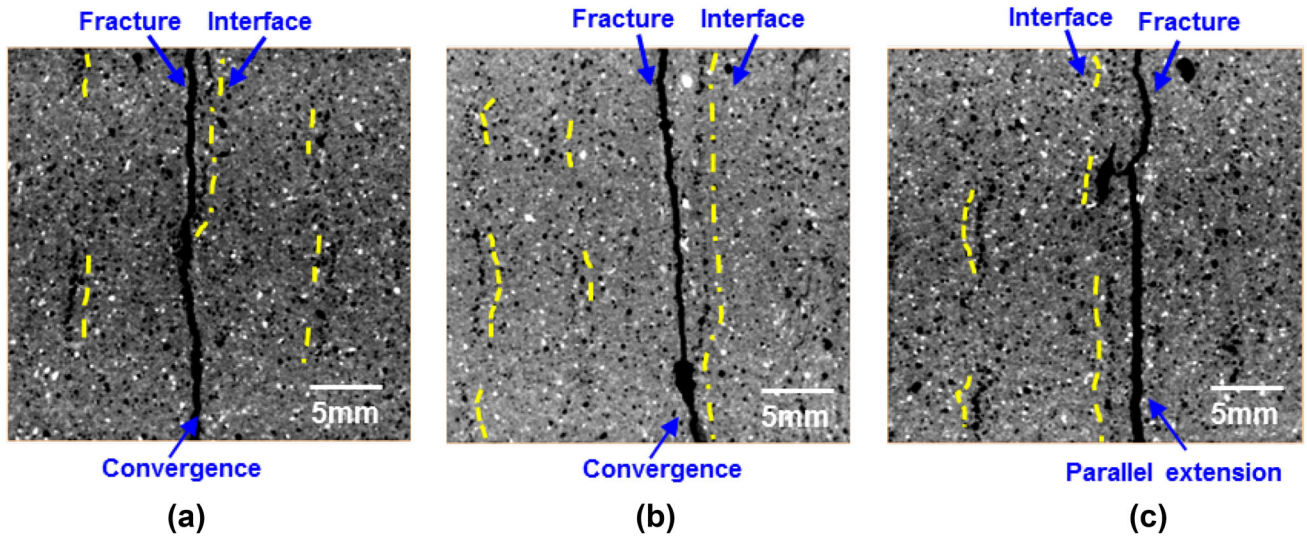
Fig. 10 CT images characterizing the microscale structures in neighbourhood of the bending fractures of specimens incorporating a content of **a** 0.5%, **b** 1.0%, and **c** 1.5% VMA.

can be normal, parallel or cross layer structures. From these measured results, it is feasible and promising to employ proper viscous modify agent for the material preparation to reach desirable structural performances.

3.5 Effect of Curing Method on the Bending Behaviour

Due to the layered build-up manner, 3D printing of cementitious material is appropriate for prefabricated structural components. Proper curing can promote the strength development of the concrete structures. Figure 11 evaluates the bending behaviour of prism specimens cured through standard curing method, water curing method and steam
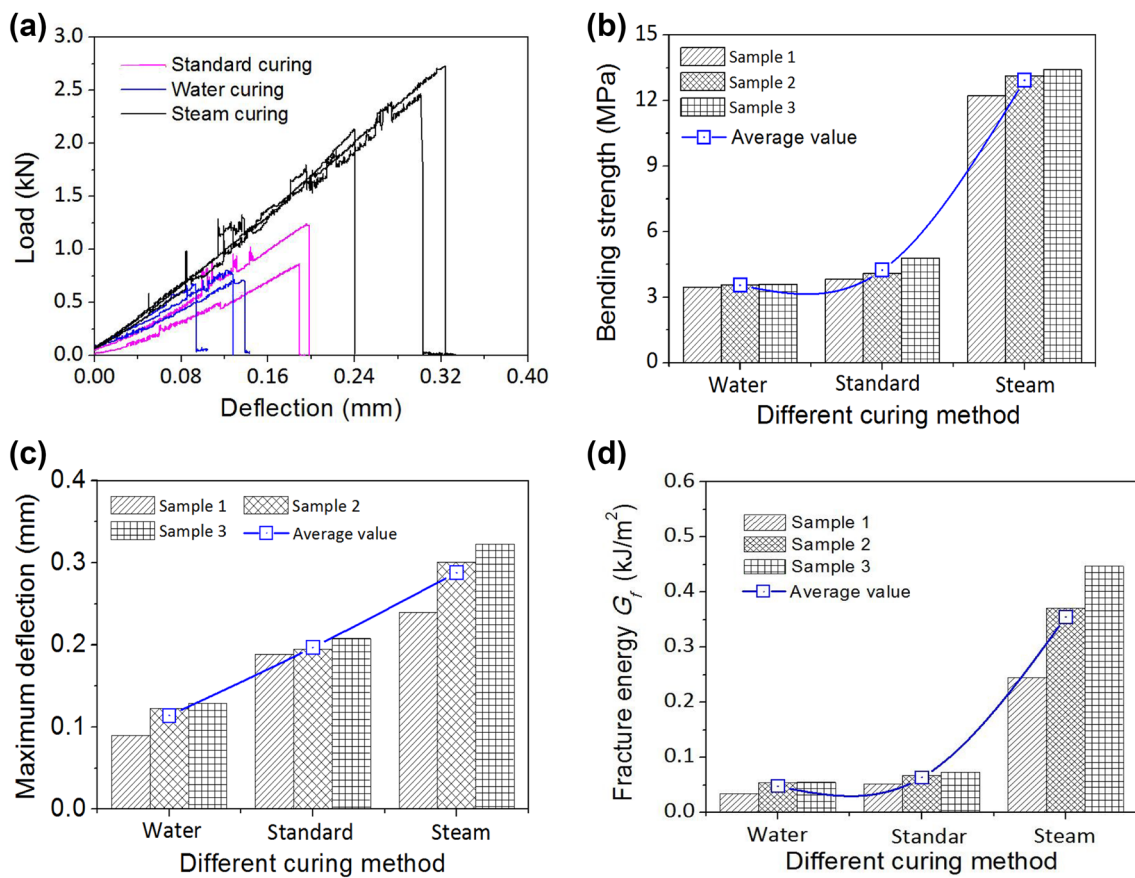
Fig. 11 Evaluation of the flexural behaviour of prism specimen cured with different method. **a** Load–deflection curves, **b** flexural strength, **c** maximum deflection, and **d** fracture energy of prism specimens.

curing method. From these test results, the distinct brittleness of mortar material has not been modified through the different curing method. The beam specimens instantly fractured once the peak load was reached (Fig. 11a). As the measured results given in Fig. 11b, the bending strength of standard cured specimens are close to the water cured ones. However, the 90 °C steam curing manner significantly enhanced the strength development. The flexural strength of specimens with steam curing was about four times higher than that of the standard curing. Steam curing improves the maximum mid-span deflection of specimens about 50% relative to the standard cured samples. These findings are mainly derived from that silica fume reacts with the calcium hydroxide ($Ca(OH)_2$) during the hydration of cement and promotes the formation of calcium silicate hydrates (C–S–H). This phase links the various components together allows to create a dense and compact cementitious matrix, resulting in a high mechanical properties (Ju et al. 2013).

From the test results, steam curing significantly contributes to the improvement of the microstructures of the cement matrix as well as elimination of the interlayer delamination, therefore resulting in the structural capacity enhancement of the printed structures. While this is sufficient for some construction applications, further improvements to strength will be necessary for many construction applications.

4. Conclusions

This paper has investigated the structural capacity of components printed at a favourable buildability situation. The paste age, VMA content and curing method are considered to optimize the buildability of the fresh paste and the mechanical strength of the hardened material to meet the requirements and demands of structural capacity of the printed stricture. The following conclusions can be drawn from this study:

(1) As a result, the buildability of the proposed tailing material can be controlled by adjusting the paste age. The longer the paste age, the better the buildability. At the paste age of 45 min, the average layer thickness measures for 75 mm, accounting for 93.8% of the optimal designed value. The Low-slump characteristic represents a well buildability. It is feasible to improve the buildability by adjusting the paste age.

(2) The flexural strength f_{flx} of specimens printed at the paste age of 45 min accounts for 46.1% of the mould-casted samples. From the CT identification, the weak bonding interface are characterized by discontinuously distributed small voids along the boundary of extruded filaments. The weak interface becomes more noticeable as the paste age increases. The inherent nature of layer delamination negatively influences the structural integrity and capacity of printed models.

(3) Incorporating a content of 1.5% viscous modify agent can increase the flexural strength and fracture energy by 25 and 54.5%, respectively. The addition of VMA eliminate the influence of the interlayer delamination on the fracture path to a large extent. The flexural strength of material with 1.5% VMA measures 67% of the mould-casted ones. The flowability of fresh paste shall be taken into account to meet the basic requirement of a desirable printability when a certain amount of VMA is adopted.

(4) Steam curing method introduced in this study increased the strengths approximately four times from the original strength. Flexural strengths about 12.93 MPa can be achieved with this post-processing method. The inherent nature of the layered structure becomes less distinct as components are cured. Heat curing at 90 °C may not be an applicable means for the rapid manufacturing processing, however, it is indeed a promising post-treatment method for enhancing the mechanical performances.

The paper has investigated the structural integrity and bending resistance of the components printed at a favourable buildability situation. It is applicable and favourable to enhance the 3D printed structures by the proposed methods. However, there still exist certain mechanical mismatch between the printed with mould-cast specimens. Next step researches shall be continuously explored to reduce the weakening impact of layer delamination on the structural performance of components. Meanwhile, the mechanical anisotropy of the printed laminar structure is necessary to be investigated in the ongoing works. Since the current printed objects are either unreinforced, or reinforcement is applied manually, fibre reinforced cement mixtures or fibre-reinforced polymers (FRPs) that is of great potential to increases the ductility of the printed mortar should be developed. Further research will also be devoted to explore the frontiers of 3D printing and promote its effective application in the real-life construction sectors.

References

ASTM C348-14. (2014). Standard Test Method for Flexural Strength of Hydraulic-Cement Mortars, ASTM International, West Conshohocken, PA. www.astm.org.

Attaran, M. (2017). The rise of 3-D printing: The advantages of additive manufacturing over traditional manufacturing. *Business Horizons, 60*(5), 677–688.

Benaicha, M., et al. (2015). Influence of silica fume and viscosity modifying agent on the mechanical and rheological behavior of self compacting concrete. *Construction and Building Materials, 84,* 103–110.

Boumiz, A., Vernet, C., & Tenoudji, F. C. (1996). Mechanical properties of cement pastes and mortars at early ages: Evolution with time and degree of hydration. *Advanced Cement Based Materials, 3,* 94–106.

Buswell, R. A., et al. (2007). Freeform construction: Mega-scale rapid manufacturing for construction. *Automation in Construction, 16*(2), 224–231.

Cesaretti, G., et al. (2014). Building components for an outpost on the Lunar soil by means of a novel 3D printing technology. *Acta Astronautica, 93,* 430–450.

Feng, L., & Liang, Y. (2014). Study on the status quo and problems of 3D printed buildings in China. *Global Journal of Human Social Science, 14,* 7–10.

Feng, P., et al. (2015). Mechanical properties of structures 3D printed with cementitious powders. *Construction and Building Materials, 93,* 486–497.

Gallucci, E., et al. (2007). 3D experimental investigation of the microstructure of cement pastes using synchrotron X-ray microtomography (μCT). *Cement and Concrete Research, 37*(3), 360–368.

Gibbons, G. J., et al. (2010). 3D Printing of cement composites. *Advances in Applied Ceramics, 109*(5), 287–290.

Gosselin, C., et al. (2016). Large-scale 3D printing of ultra-high performance concrete—a new processing route for architects and builders. *Materials and Design, 100,* 102–109.

Hambach, M., & Volkmer, D. (2017). Properties of 3D-printed fiber-reinforced Portland cement paste. *Cement and Concrete Composites, 79,* 62–70.

Ju, Y., et al. (2013). An investigation on micro pore structures and the vapor pressure mechanism of explosive spalling of RPC exposed to high temperature. *Science China Technological Sciences, 56*(2), 458–470.

Ju, Y., et al. (2017a). Visualization of the three-dimensional structure and stress field of aggregated concrete materials through 3D printing and frozen-stress techniques. *Construction and Building Materials, 143,* 121–137.

Ju, Y., et al. (2017b). Visualization and transparentization of the structure and stress field of aggregated geomaterials through 3D printing and photoelastic techniques. *Rock Mechanics and Rock Engineering, 50*(6), 1383–1407.

Kazemian, A., et al. (2017). Cementitious materials for construction-scale 3D printing: Laboratory testing of fresh printing mixture. *Construction and Building Materials, 145,* 639–647.

Khoshnevis, B. (2004). Automated construction by contour crafting—related robotics and information technologies. *Automation in Construction, 13*(1), 5–19.

Khoshnevis, B., & Dutton, R. (1998). Innovative rapid prototyping process makes large sized, smooth surfaced complex shapes in a wide variety of materials. *Materials Technology, 13*(2), 53–56.

Kovler, K., & Jensen, O. M. (2005). Novel techniques for concrete curing. *Concrete International, 27,* 39–42.

Labonnote, N., et al. (2016). Additive construction: State-of-the-art, challenges and opportunities. *Automation in Construction, 72,* 347–366.

Lachemi, M., et al. (2004). Performance of new viscosity modifying admixtures in enhancing the rheological properties of cement paste. *Cement and Concrete Research, 34*(2), 185–193.

Le, T. T., et al. (2012a). Hardened properties of high-performance printing concrete. *Cement and Concrete Research, 42*(3), 558–566.

Le, T. T., et al. (2012b). Mix design and fresh properties for high-performance printing concrete. *Materials and Structures, 45*(8), 1221–1232.

Leemann, A., & Winnefeld, F. (2007). The effect of viscosity modifying agents on mortar and concrete. *Cement and Concrete Composites, 29*(5), 341–349.

Lim, S., et al. (2012). Developments in construction-scale additive manufacturing processes. *Automation in Construction, 21,* 262–268.

Lin, S. T., & Huang, R. (2010). Effect of viscosity modifying agent on plastic shrinkage cracking of cementitious composites. *Materials and Structures, 43*(5), 651–664.

Lu, S., Landis, E. N., & Keane, D. T. (2006). X-ray microtomographic studies of pore structure and permeability in portland cement concrete. *Materials and Structures, 39*(290), 611–620.

Ma, G., Li, Z., & Wang, L. (2018). Printable properties of cementitious material containing copper tailings for extrusion based 3D printing. *Construction and Building Materials, 162,* 613–627.

Ma, G., & Wang, L. (2017). A critical review of preparation design and workability measurement of concrete material for largescale 3D printing. *Frontiers of Structural Civil Engineering, 6,* 1–19.

Panda, B., et al. (2017). Measurement of tensile bond strength of 3D printed geopolymer mortar. *Measurement, 113,* 108–116.

Pegna, J. (1997). Exploratory investigation of solid freeform construction. *Automation in Construction, 5*(5), 427–437.

Perrot, A., Rangeard, D., & Melinge, Y. (2015). Prediction of the ram extrusion force of cement-based materials. *Applied Rheology, 24*(5), 53320.

Perrot, A., Rangeard, D., & Pierre, A. (2016). Structural built-up of cement-based materials used for 3D-printing extrusion techniques. *Materials and Structures, 49*(4), 1213–1220.

Perrot, A., et al. (2006). Ram extrusion force for a frictional plastic material: Model prediction and application to cement paste. *Rheologica Acta, 45*(4), 457–467.

Perrot, A., et al. (2012). Use of ram extruder as a combined rheo-tribometer to study the behaviour of high yield stress fluids at low strain rate. *Rheologica Acta, 51*(8), 743–754.

Reinhardt, H. W., & Grosse, C. U. (2004). Continuous monitoring of setting and hardening of mortar and concrete. *Construction and Building Materials, 18*(3), 145–154.

Rudenko, A. (2015). 3D concrete house printer. http://www.designboom.com/technology/3d-printed-concrete-castle-minnesota-andrey-rudenko-08-28-2014/.

Trtnik, G., et al. (2008). Possibilities of using the ultrasonic wave transmission method to estimate initial setting time of cement paste. *Cement and Concrete Research, 38*(11), 1336–1342.

Voigt, T., Akkaya, Y., & Shah, S. P. (2003). Determination of early age mortar and concrete strength by ultrasonic wave reflections. *ournal of Materials in Civil Engineering, 15*(3), 247–254.

Voigt, T., Malonn, T., & Shah, S. P. (2006). Green and early age compressive strength of extruded cement mortar monitored with compression tests and ultrasonic techniques. *Cement and Concrete Research, 36*(5), 858–867.

WASP. (2016). The first adobe building. http://www.wasproject.it/w/en/3d-printers-projects/, 2016.

Winsun. (2015). WinSun China builds world's first 3D printed villa and tallest 3D printed apartment building. http://www.3ders.org/articles/20150118-winsun-builds-world-first-3d-printed-villa-and-tallest-3d-printed-building-in-china.html.

Zhang, J., & Khoshnevis, B. (2013). Optimal machine operation planning for construction by Contour Crafting. *Automation in Construction, 29,* 50–67.

Zhang, M., et al. (2012). Computational investigation on mass diffusivity in Portland cement paste based on X-ray computed microtomography (μCT) image. *Construction and Building Materials, 27*(1), 472–481.

Zhao, Z., Kwon, S. H., & Shah, S. P. (2008). Effect of specimen size on fracture energy and softening curve of concrete: Part I. Experiments and fracture energy. *Cement and Concrete Research, 38*(8), 1049–1060.